Hellenic Strong-Motion Database with Uniformly Assigned Source and Site Metadata for the Period 1972–2015

Basil Margaris[1], Emmanuel M. Scordilis[2] , Jonathan P. Stewart[*3] , David M. Boore[4] , Nikos Theodoulidis[1], Ioannis Kalogeras[5], Nikolaos S. Melis[5] , Andreas A. Skarlatoudis[6] , Nikolaos Klimis[7] , and Emel Seyhan[8]

Abstract

We present a Hellenic database of intensity measures from uniformly processed strong ground motion recordings, together with metadata on earthquake source attributes and recording site conditions. The database consists of information from 471 earthquakes between 1973 and 2015 that produced 2993 usable recordings from 333 sites. A key element of this work is a unified presentation of data from two major data providers that operate in Greece (Institute of Engineering Seismology and Earthquake Engineering and the Institute of Geodynamics, National Observatory of Athens) along with a university-operated local urban array (University of Patras). Consistent procedures were applied to develop source parameters that include hypocenter locations, moment magnitudes (directly estimated or derived using a conversion procedure), fault-plane solutions, and finite-fault parameters (generally, for events with M > 6.0). The time-averaged shear-wave velocity in the upper 30 m parameter is provided for all 333 recording sites based on geophysical measurements where available (102) and proxy-based estimates otherwise. Most events are in the magnitude range of 3.8–7, occurred at shallow hypocentral depths (< 30 km), and provide data for rupture distances generally between 10 and 300 km. The combined ground motion, seismic source, and site database is anticipated to be useful for engineering applications, including ground-motion model development and time series selection for response-history analyses.

Introduction

The well-known Next Generation Attenuation (NGA) projects compile global ground-motion data from different regions for application to particular tectonic regimes, such as, active tectonic regions, subduction zones, and stable continental regions (Bozorgnia *et al.*, 2014; Goulet *et al.*, 2014; Pacific Earthquake Engineering Research [PEER], 2020). Ground-motion time series are processed in a uniform manner, intensity measures are computed (such as peak acceleration, pseudospectral accelerations, and durations), and metadata are derived in a consistent way for use in ground-motion prediction equation (GMPE) development and other engineering applications. Global databases of this sort inevitably rely on a series of local or regional databases, which have varying levels of documentation and consistency. This article presents the results of over a decade of work to compile, uniformly process, and systematically document a ground-motion database for active

tectonic shallow-crustal earthquakes in Greece. The database has three major components: (1) uniformly processed strong-motion accelerograms and their intensity measures, (2) metadata describing site conditions at accelerometer sites, and (3) metadata on earthquake source parameters. The tables

1. ITSAK—Institute of Engineering Seismology and Earthquake Engineering, Thessaloniki, Greece; 2. AUTh: Aristotle University of Thessaloniki, Geophysical Laboratory, Aristotle University, Thessaloniki, Greece, https://orcid.org/0000-0001-7350-9498 (EMS); 3. University of California, Los Angeles, Los Angeles, California, U.S.A., https://orcid.org/0000-0003-3602-3629 (JPS); 4. Seismologist, Los Altos, California, U.S.A., https://orcid.org/0000-0002-8605-9673 (DMB); 5. National Observatory Athens—Institute of Geodynamics, Athens, Greece, https://orcid.org/0000-0002-8966-4449 (NSM); 6. AECOM, Los Angeles, California, U.S.A., https://orcid.org/0000-0003-1823-4617 (AAS); 7. Democritus University of Thrace (DUTh), Xanthi, Greece, https://orcid.org/0000-0001-9770-2583 (NK); 8. Risk Management Solutions, Inc., Newark, California, U.S.A.

*Corresponding author: jstewart@seas.ucla.edu

compiled for this study are provided as files in the supplemental material included with this article.

The present database builds upon earlier work, which began in the 1973 with a strong-motion instrumentation project within the framework of a project entitled "Balkan region seismicity study" (Berckhemer and Hsu, 1982). Major advances in the deployment and advancement of ground-motion instruments occurred in different time periods (1982–1984, 1999–2002, and 2009–2013), as described in Margaris et al. (2014). At present, the principal ground-motion monitoring networks operating in Greece are the Institute of Engineering Seismology and Earthquake Engineering–Earthquake Planning and Protection Organization (ITSAK-EPPO), National Observatory of Athens—Geodynamic Institute (NOA-IG), and some other local networks (e.g., U_Patras: Civil Engineering Department at the University of Patras). As part of this project, a consortium of these networks has been recently established, which is referred to as the Hellenic Accelerographic Networks (HANs).

The most significant prior compilation of Hellenic data across networks was the homogeneous HEllenic Accelerogram Database (HEAD) initiated by Theodoulidis et al. (2004). The HEAD database had 677 three-component ground motions from 319 events for moment magnitudes of 4–7 and distances up to 160 km. A subset of the HEAD data was included in a European database by Ambraseys et al. (2000); Ambraseys, Douglas, et al. (2004); and Ambraseys, Smit, et al. (2004). The full HEAD database was incorporated into the Earthquake Strong Motion (ESM) database by Luzi et al. (2016). The ITSAK-EPPO portion of the HEAD database was subsequently modified using a Geographic Information System access portal and supplemented to include data up to 2015. This database, referred to as GHEAD, has 1097 three-component ground motions from 401 earthquakes ranging in moment magnitude from 4 to 7. That inventory of Greek data from ITSAK-EPPO stations was reprocessed for GHEAD, as described in Margaris et al. (2014).

The present effort has expanded the database to include events through 2015 and systematically improved metadata quality, particularly, in reference to source parameters (moment tensors, finite-fault parameters, and event classifications as foreshock–mainshock–aftershock) and site parameters (consistent geologic descriptions and assignment of time-averaged shear-wave velocity in upper 30 m, V_{S30}). As presented here, the Hellenic database has 2993 three-component ground motions from 471 earthquakes over a moment magnitude range of 3.8–7.0. Our objective in this article is to describe the new Hellenic strong-motion database and procedures used to compile and configure the data. The parameter space covered by the data is presented, and limitations of the data relative to other European or international databases (Ancheta et al., 2014; Luzi et al., 2016) are described. This work was undertaken in support of a project to develop a NGA-quality ground-motion database for Greece, suitable for the derivation of pertinent regional GMPEs. The development

of ground-motion models from this data is the subject of a separate article (Boore et al., 2020).

Earthquake Source Table

The source table contains explanatory event data (name, origin date, and time), hypocenter location, magnitude, fault-plane solutions (FPSs, as derived from moment tensors), information on focal mechanism, event-type classifications (i.e., foreshock, mainshock, or aftershock), finite-fault parameters (where available), and references. In the following sections, we describe procedures used to select source parameters. In this study, events with focal depth $h \leq 60$ km are considered, which should encompass, essentially, all shallow-crustal earthquakes, but likely includes some subduction events as well (Papazachos and Comninakis, 1971; LePichon and Angelier, 1979). The source table is provided as Table S1 in the supplemental material.

Earthquake locations

We consider sources within the broader Aegean region bounded by 33°–43° N and 18°–31° E and events with focal depths less than 60 km. The depth threshold was motivated by the Benioff subduction zone in Greece, which starts at approximately 60 km depth, and our intention in the present work to include as many shallow-crustal earthquakes as possible. We acknowledge that some subduction events are likely included among the data, and we have not attempted to remove data from such events. To ensure the exclusion of subduction events, users may wish to apply shallower depth thresholds in event selection (e.g., <30 km). The main sources of earthquake locations (epicentral coordinates and focal depths) were online International Seismological Centre (ISC) bulletins. ISC locates earthquakes by gathering and incorporating phase readings from many national networks. Its bulletins are homogeneous and sufficiently accurate for our purposes.

For events not listed in ISC bulletins, the catalog was completed with data from various sources listed in Data and Resources. Where improved locations are provided in published research, they were adopted (e.g., Bernard et al., 1997; Papazachos and Papazachou, 2003; Galanis, 2010; Karakostas et al., 2017).

Hypocentral depths from ISC bulletins and local sources can differ, mainly because the latter can use local recordings of both P and S waves, which have the potential to refine event locations. Figure 1 shows hypocentral depths differentiated by the information source from which they were taken. For $\mathbf{M} > 5.5$ events, we do not see systematic differences based on information source. For $\mathbf{M} < 5.5$ events, the local sources tend to be shallower than those for ISC for small magnitudes. Although, the consistent use of local sources would be preferred across all events, this was not possible in the present work, and we have not modified hypocentral depths from those provided in source documents.
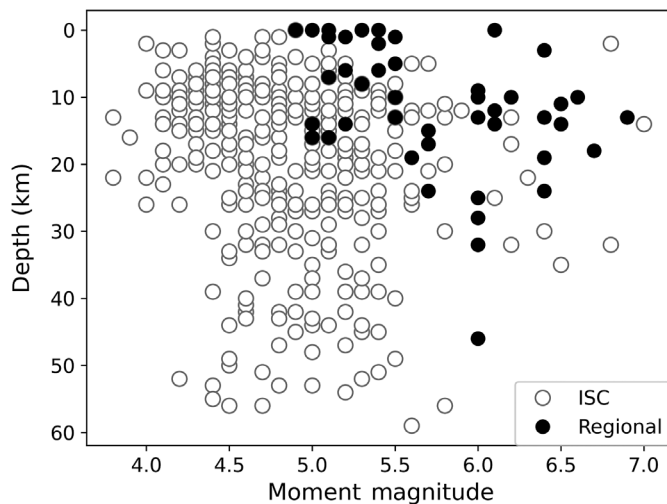
Figure 1. Hypocentral depth distribution of events with respect to magnitude. ISC, International Seismological Centre.

The column of the source table in the supplemental material entitled "References—Focus" provides information on the sources of the focal parameters that were adopted in the final catalog. The code numbers of the respective references are listed in a tab of the source table file.

Magnitude

A common problem in compiling earthquake catalogs is providing consistent magnitudes. The bulletins and catalogs used for source locations (prior section) provide magnitudes in different scales (surface-wave magnitude [M_s], body-wave magnitude [m_b], local magnitude [M_L], duration magnitude [M_D], and moment magnitude [$\mathbf{M}$]). We adopted the moment magnitude scale, $\mathbf{M}$ (Hanks and Kanamori, 1979), as the reference, which is consistent with NGA and similar database standards. For events without an available moment magnitude, other magnitude types were compiled and then converted to moment magnitude using each of a series of conversion equations (Papazachos et al., 1997; Baba et al., 2000; Scordilis, 2005, 2006; Tsampas, 2006; Duni et al., 2010).

The seismic moments in the source table are taken directly from original documents. In order of preference, we use Global Centroid Moment Tensor (Global CMT; Dziewonski et al., 1981; Ekström et al., 2012), U.S. Geological Survey (USGS), Papazachos and Papazachou (2003), and Konstantinou (2015). We recognize that there can be differences between seismic moments published by different agencies for a given event, which contribute epistemic uncertainties to magnitude assignments. These uncertainties impact between-event variability in ground-motion models derived from the data, although, the effects in the case of magnitude uncertainties have been shown to be small (Kuehn and Abrahamson, 2018). Systematic differences in seismic moments and $\mathbf{M}$-values from our

principal global sources (Global CMT and USGS) across a catalog of events in the study region are small (about 0.06; Gasperini et al., 2012). We elected not to adjust published magnitudes to a common reference, given the lack of consensus on the need for doing so (e.g., such adjustments are not made in NGA projects) and the potential for creating confusion in which our magnitudes do not match those in source documents.

Where conversions are applied from several other magnitude scales for a given event, the equivalent moment magnitude is taken as the weighted mean of converted magnitudes. The weights used in the analysis are proportional to the inverse standard deviations of the respective magnitude conversion equations.

FPSs

We have included in the source table information on fault type (i.e., dip slip or strike slip, normal or thrust, dextral or sinistral), which is used in GMPEs for active tectonic regions to define style of faulting parameters. Such information is available from FPSs. Where available, we use FPS from Global CMT maintained by the Lamont–Doherty Earth Observatory of Columbia University.

The Global CMT online catalog provides FPS information only for moderate-to-strong earthquakes. Information for smaller events was collected from:

1. Local, seismological centers (such as Aristotle University of Thessaloniki, NOA, European-Mediterranean RCMT (MED_RCMT), ETH Zurich RMT (ZUR_RMT), etc.; see Table 1).
2. Publications or reports on studies of specific earthquakes.
3. Review studies of FPSs and the stress field in the broader area of Greece.

References for FPSs are given in Table S1 (under the column "References–FPS").

The information provided in the source table in the supplemental material includes the following information for each of the two nodal planes (NP1 and NP2):

- Plane strike angle, expressed as the azimuth from North (Az1/Az2),
- Plane dip angle (Dp1/Dp2), and
- Rake angle (Rk1/Rk2).

We have high confidence in NP1 as the rupture plane, when it aligns with the strike of the causative fault; such cases are labeled as "C" (confident) in the column "NP_Pref" of the source table in the supplemental material. In other cases, NP1 is probable as the rupture plane, but the lower confidence is marked with "P" in NP_Pref. References documenting the basis for assigning an earthquake to a particular fault are given

TABLE 1
Sources of Focal Parameters and Fault-Plane Solution (FPS) Information

Center	Web Address
AUTh	http://geophysics.geo.auth.gr/the_seisnet/WEBSITE_2005/station_index_en.html
Global CMT	http://www.globalcmt.org/
ISC	http://www.isc.ac.uk
KOERI	http://www.koeri.boun.edu.tr/sismo/2/moment-tensor-solutions/ and http://www.emsc-csem.org/Earthquake/tensors.php
MED_RCMT	http://www.bo.ingv.it/RCMT/
INGV	http://mednet.rm.ingv.it/quick_rcmt.php
NOA	http://bbnet.gein.noa.gr/HL/index.php
UPSL	http://www.emsc-csem.org/Earthquake/tensors.php
USGS	https://earthquake.usgs.gov/earthquakes/search/#{
ZUR_RMT, ETHZ	http://www.seismo.ethz.ch/static/mti/
GDDA-ERD	https://deprem.afad.gov.tr/faycozumleri

AUTh, Aristotle University of Thessaloniki; ETHZ, Eidgenössische Technische Hochschule Zürich; GDDA-ERD, General Directorate of Disaster Affairs, Earthquake Research Department; Global CMT, Global Centroid Moment Tensor; INGV, Istituto Nazionale di Geofisica e Vulcanologia; ISC, International Seismological Centre; KOERI, Kandilli Observatory and Earthquake Research Institute; NOA, National Observatory of Athens; UPSL, University of Patras Seismological Laboratory; USGS, U.S. Geological Survey. All websites were last accessed in February 2021.

in the last column of source table (column "References—FP"). In some cases, alternative interpretations suggest fault characteristics deviating from those of NP1; where applicable, the alternative interpretations and the associated references are also given in the column "References—FP Comments." For some strong aftershocks with unknown fault planes, nodal planes with characteristics similar to those of the mainshock were adopted.

Rake angles were obtained from the aforementioned moment tensor solutions and are reported in the source table. Also provided are the P plunge and T plunge (e.g., Aki and Richards, 1980). Discrete assessments of focal mechanism (1 = strike slip, 2 = normal slip, 3 = reverse slip) are provided in separate columns based on the plunge of the mechanism, when available, and otherwise on the rake of the slip on the fault plane (see appendix D in Boore and Atkinson, 2007, for details).

Event declustering
The source table includes 497 earthquakes. Some of these earthquakes are mainshocks, but there are also events belonging to aftershock or foreshock sequences as well as some "independent" events (events not identified as foreshocks or aftershocks by the declustering algorithm, as well as events with no

foreshocks or aftershocks of their own). We apply declustering to an expanded version of the catalog, to separate events by source type (foreshock, mainshock, or aftershock). The expanded version of the event catalog incorporated events for which there are no strong motion data for the same spatial window (33°–43° N and 18°–31° E) and the time period 1970–2015. This expanded catalog was declustered, and the event classifications were transferred to the catalog of 471 events with available strong-motion records.

We used a declustering procedure that distinguishes event types based on relations connecting the dimension of the seismogenic region surrounding a mainshock and the duration of the aftershocks sequence with the moment magnitude for the mainshock. The adopted relations are:

$$\log d = 0.124\mathbf{M} + 0.983, \tag{1}$$

$$\log T = 0.66\mathbf{M} - 2.08. \tag{2}$$

Equation (1) was proposed by Gardner and Knopoff (1974) and provides the radius, d (in kilometers), of a circle centered on the epicenter of a mainshock of magnitude $\mathbf{M}$ that delimits the seismogenic region of the sequence. Equation (2), proposed by Papazachos and Papazachou (2003), depicts the duration, T (in days) of the aftershock sequence, starting from the origin time of the mainshock, as a function of mainshock magnitude $\mathbf{M}$. We consider a foreshock period of one month prior to the mainshock.

To decluster the catalog, we first identified the strongest earthquake, which was taken as a mainshock ($\mathbf{M}$). Then, its possible foreshocks (f) and aftershocks (a) were defined by applying equations (1) and (2). This procedure was repeated for the second strongest event (after removing the events of the first sequence), and, so forth, until all the earthquakes in the catalog were characterized (see Fig. 2). We only consider events as mainshocks if they have magnitudes $\mathbf{M} \geq 5.0$.

The results of applying this procedure are that the source database contains 153 mainshocks, 37 foreshocks, 143 aftershocks, and 138 "independent" events. The event categories are indicated in the source table as foreshocks (f), mainshocks (M), and aftershocks (a) in the column "Seq $f/M/a$."

Finite-fault solutions
Finite-fault models describe the earthquake source geometry in terms of a plane or series of planes that delineate the portions of a fault that produced fault slip significantly contributing to earthquake ground motions. The geometric representation of the finite-fault geometry is important for the measurement of rupture distance (closest distance to fault plane) and Joyner–Boore distance (closest distance to surface projection of rupture plane), as well as for resolving the location of a site with respect to the hanging wall of the fault.
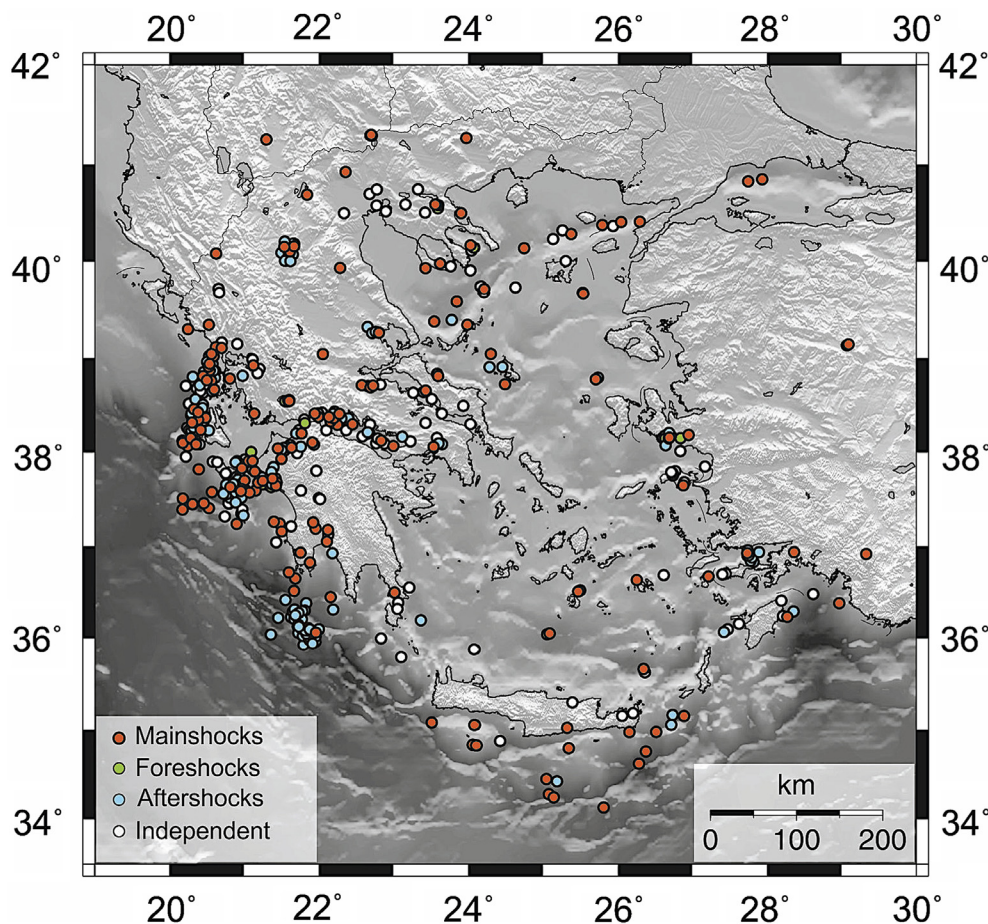
Figure 2. Map of epicenters of the earthquakes included in source table. Red, green, cyan, and white circles stand for mainshocks, foreshocks, aftershocks, and "independent" events, respectively. The color version of this figure is available only in the electronic edition.

hypocentral distance, R_{HYP}; closest distance to rupture plane, R_{RUP}; closest distance to surface projection of rupture plane, also known as Joyner–Boore distance, R_{JB}; distance measured perpendicular to the fault strike from the surface projection of the up-dip edge of the fault plane, R_x; distance measured parallel to the fault strike from the midpoint of the surface projection of the fault plane, R_y; and distance measured parallel to the fault strike from the end of the surface projection of the fault plane, R_{y0}.

For events without a published finite-fault solution, we applied a simulation approach to develop an approximate finite-fault model to compute distance parameters based on the earthquake magnitude, style of faulting, strike and dip angles, and regional relationships for fault length (along strike) and width (down-dip). The methodology for simulating the fault plane consists of random sampling of probabilistic distributions of fault-rupture area, aspect ratio of ruptured area, and hypocenter position on the fault plane. The methodology was introduced in appendix B of Chiou and Youngs (2008) and subsequently updated, better documented, and refined by Contreras et al. (2020). The method involves the use of scaling relationships between moment magnitude and rupture area, R_A (km²), length, L_R, and width, W_R, of the rupture. We used Greek relations (Papazachos et al., 2004) for the scaling of fault area, length, and width with moment magnitude in tectonically active regions. These procedures were used for all events not listed in Table 2. Distance parameters derived from this process are given in the flatfile (Table S3), with the exception of events without an identified focal mechanism or depth >40 km.

Literature searches were undertaken to identify finite fault models for significant Hellenic events, generally having $\mathbf{M} \geq 6$. When multiple models were available, preference was given to models derived from field observations of coseismic surface rupture, the coseismic slip distribution (derived from inversion of waveforms and/or from geodetic data), and the spatial distribution of aftershocks. The events for which finite-fault solutions have been included in the database are listed in Table 2, along with the finite-fault geometric attributes assigned to the rupture. Among the collected parameters are the geographic coordinates and the depth of the upper-left corner (ULC) of the fault plane (because it is observed from the hanging wall), as well as the strike, dip, along-strike length, and down-dip width of the rupture.

Analysis of site-to-source distance

The distance measures included in the database are calculated based on the geometry of the finite-fault rupture plane and the location of the station. Seven source-to-site distance measures are included in the database: epicentral distance, R_{EPI};

Site Attributes
Instruments

From the onset of the strong-motion instrumentation program in Greece through the late 1990s, the majority of the installed accelerographs consisted of analog SMA-1 units. The deployment of low-resolution digital instruments (initially

TABLE 2
Information on Available Finite-Fault Solutions for Strong (M≥6.0) Earthquakes

Earthquake ID	Year	Region	M	References	Number of Recordings	L (km)	W (km)	Z_{tor} (km)	Strike (°)	Dip (°)	ULC Latitude	ULC Longitude	Comments
1509	1981	Alkyonides	6.7	8, 23	1	31	15	0	285	37	38.057	22.999	
1540	1986	Kalamata	6.0	13, 10	2	15	11	2	**201**	**45**	37.130	22.225	
1556	1988	Kyllini	6.0	21	5	16	12	3	338	48	37.847	21.022	
1608	1994	North Macedonia	6.1	8	1	15	10		343	49			Limited data
1619	1995	Kozani	6.5	14	6	30	15	5	**252**	**41**	40.100	21.710	
1633	1995	Aegion	6.4	3	8	15	9	5	277	33	38.270	22.317	Also L = 24
1649	1997	Kalamata	6.4	8	4	21	23	5	298	20			Limited data
1670	1999	Athens	6.0	15, 11, 12	12	12	14	5	**114**	**45**	38.12	23.53	
1059	2001	Skyros	6.4	16	3	30	25	0	148	76	39.18	24.15	
859	2003	Lefkada	6.2	1, 2	12	22	13	10	**16**	**72**	38.650	20.550	
130	2008	South of Peloponessus	6.8	17, 6	6	30	20	6	332	6	36.299	21.811	
217	2008	Achaia-Ilia	6.4	7	36	22	13	12	209	83	38.090	21.620	
1700	2012	Turkey	6.2	4	60	24	12	16	206	72	36.4847	28.8821	
1707	2013	Crete	6.3	5	36		18	2	**283**	**33**			Limited data
1708	2013	Crete	6.1	5	78			2	**46**	**77**			Limited data
1713	2014	Cephalonia #1	6.1	20	43	27	10	0.5	**20**	**80**	38.19	20.38	
1715	2014	Cephalonia #2	6.0	20	126	35	10	0	**199**	**49**	38.3339	20.4186	
1718	2014	North Aegean	6.9	18	60	58	20	0	75	85	40.2593	25.2279	
1731	2015	Crete–Karpathos	6.1	9	141	25	17	4	**75**	**40**	35.25	26.5	
1736	2015	Lefkada	6.5	19	148	24	13	3	**10**	**70**	38.4657	20.501	

Values in boldface are modified from the source table in the supplemental material based on references used for finite-fault models. ULC, upper-left corner.

(1) Benetatos et al. (2005); (2) Benetatos et al. (2007); (3) Bernard et al. (1997); (4) Dogan et al. (2016); (5) Gorgun (2017); (6) Howell et al. (2017); (7) Karakostas et al. (2017); (8) Karakaisis et al. (2010); (9) Kiratzi (2016); (10) Lyon–Caen et al. (1988); (11) Papadimitriou et al. (2002); (12) Papadopoulos et al. (2000); (13) Papazachos et al. (1988); (14) Rigo et al. (2004); (15) Roumelioti et al. (2003); (16) Roumelioti et al. (2004); (17) Roumelioti et al. (2009); (18) Saltogianni et al. (2016); (19) Saltogianni et al. (2017); (20) Sokos et al. (2015); (21) Karakostas et al. (1993); (22) Carver and Bollinger (1983); (23) Papazachos et al. (1984).

Kinemetrics SSA2; later 11-bit Kinemetrics Quake Data Recorder [QDR]) began in the mid-1990s and concluded by the end of 2001, by which time all analog units had been replaced. The number of instruments in operation at this time was 120. The dynamic range of those digital sensors and their technical specifications did not appreciably differ from their analog predecessors. However, they provided significant advantages by eliminating digitization errors, and facilitating remote maintenance and data collection.

Since 2008, several projects have increased the quantity and quality of the national strong-motion instruments within the ITSAK-EPPO and NOA-IG networks. Instruments deployed since 2010 are 24-bit CMG-5TD-EAM units, with significantly enhanced dynamic range and sensitivity, as well as capabilities for continuous monitoring and remote access to the data. In the case of ITSAK-EPPO, the prior network of 40 stations has been replaced with the newer digital instruments, and 80 additional sites have been instrumented. For NOA-IG, the prior network of 80 stations has been supplemented with 80 newer digital instruments at new sites. As of this writing, there are 380 instruments deployed by ITSAK-EPPO and NOA-IG to measure ground motion (this number does not include structural or special vertical arrays, such as EUROSEISTEST, ARGONET). These accelerographs are installed in (mainly public sector) structures of various sizes—27 are installed in relatively small instrument shelters, whereas 306 are in buildings of various sizes (approximately, 50% are 2–4 story buildings on shallow foundations, but, some are up to eight story office buildings, with one or two levels of basement). Unfortunately, a systematic compilation of information on instrument housing has not been compiled by ITSAK-EPPO and NOA-IG staff, which would be useful to evaluate the influence of soil–structure interaction effects on the recordings (e.g., Stewart, 2000). The lack of this information adds epistemic uncertainty to short-period spectral accelerations in the database.

Because there are several generations of accelerometers that have been deployed in Greece, in many cases at the same physical location (i.e., the same "site"), there is no unique relationship between "sites" and "instruments" in the present database. The word "site" indicates a physical location, and the site table contains information relevant to that location (next section). The site sequence number (SSN) is used to identify sites within the database. The instruments deployed at a site are indicated by a station code, with potentially multiple such codes used for a given SSN. For example, the site KAL (Kalamata) has had three instruments denoted KAL1, KAL2, and KAL3.

Site parameters

The primary site parameter compiled to approximately quantify site stiffness for ground motion studies is the time-averaged shear-wave velocity in the upper 30 m of the site, V_{S30}. Site parameters are only compiled for accelerograph sites that have produced usable records, which total 333 for the time period of 1972–2015. Further details on how "usable records" were identified for this purpose are provided in the Intensity Measure Calculations section.

Site parameters are compiled in a site table (Table S2 in the supplemental material). For each accelerograph site, this table contains:

- basic identifying information such as SSN, site name, and site coordinates (latitude and longitude using the WGS84 datum);
- site geology, including surface geologic descriptions and age, as taken from 1:50,000 scale geological maps (from Institute of Geology and Mine Exploration);
- site morphological information, including topographic slope based on 3 arcsec digital elevation models and terrain categories, as defined by Iwahashi and Pike (2007), which are derived from 30 arcsec digital elevation models. To define topographic slope for a given point, elevations are extracted from digital elevation models on a grid of eight points surrounding the point of interest. Slopes in all azimuths are computed using GMT software, and the maximum is taken as topographic slope;
- V_{S30} as measured from on-site geophysical measurements, where available;
- V_{S30} as estimated from various site proxies; and
- V_{S30} recommended for analysis and a code indicating the basis for its assignment.

Measured V_{S30}-values come from in situ geophysical measurements in the proximity of the station. Details on the measurement methods and the proximity of measurements to stations are provided in the profile database compiled as part of this project and provided as the supplemental material to Stewart et al. (2014). About 102 of the 333 sites have V_{S30}-values from measurements.

Estimates of V_{S30} from proxies follow procedures given in Stewart et al. (2014). In that study, empirically procedures were developed to estimate V_{S30} conditioned on two types of site proxies: (1) geomorphology-based terrain categories from Iwahashi and Pike (2007), and (2) a combination of topographic slope from 3 arcsec digital elevation models and surface geology. The surface geologic categories for which V_{S30} predictions were provided are age-based as follows: Holocene (H), Pleistocene (P), mapped undivided Quaternary (Q; used in which a more specific age is unknown), Tertiary or Neogene (T), and Mesozoic and Paleozoic (M). The two types of site proxies provide two estimates of V_{S30}, which are log averaged (equivalent to geometric mean). Because these site proxies are available for all locations in Greece, proxy-based estimates of V_{S30} are provided in the site table for all 333 sites.

The value of V_{S30} recommended for analysis is assigned using the protocols in table 5 of Stewart et al. (2014). Those protocols give preferences to V_{S30} from measurements where available, assigning various codes (0, 1, 2) to distinguish cases in
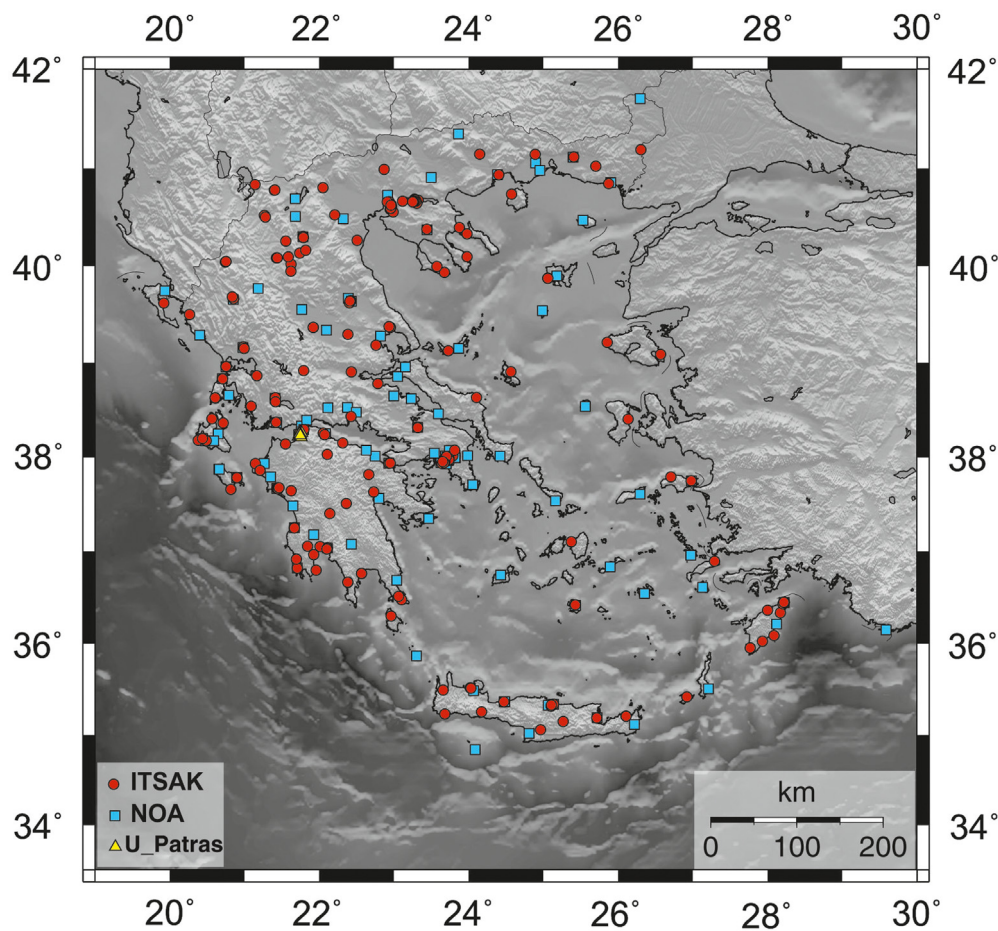
Figure 3. Spatial distribution of accelerograph sites with usable recordings. ITSAK, Institute of Engineering Seismology and Earthquake Engineering; NOA, NOA, National Observatory of Athens; U_Patras, University of Patras. The color version of this figure is available only in the electronic edition.

Figure 3 shows locations of the 333 sites with usable records and assigned V_{S30}. The sites are color coded, according to the owner of the accelerograph station. Most sites are in soil categories B and C. Figure 4 shows a histogram of the V_{S30}-values recommended for analysis. V_{S30}-based site classes are classified as in EuroCode 8 (European Committee for Standardization [CEN], 2004) as follows: $V_{S30} > 800$ m/s [class A], 361 m/s $\leq V_{S30} \leq 800$ m/s [class B], 180 m/s $\leq V_{S30} \leq 360$ m/s [class C], and $V_{S30} < 180$ m/s [class D]. The percentages of sites with measurement-based V_{S30} are as follows: A—100%, B—22%, C—44%, and D—77%. A significant majority of recordings (69%) are derived from stations with site class B. The distributions of V_{S30} and site class are similar to those reported in figure 4 of Luzi *et al.* (2016) for the ESM database (range of about 200–1000 m/s, median of approximately 400 m/s).

which the profile reaches 30 m or terminates at shallower depths, as well as cases in which the profile is located at the site or at distances up to 1.0 km from the site. Code 3 is assigned when V_{S30} is estimated from the proxy-based models.
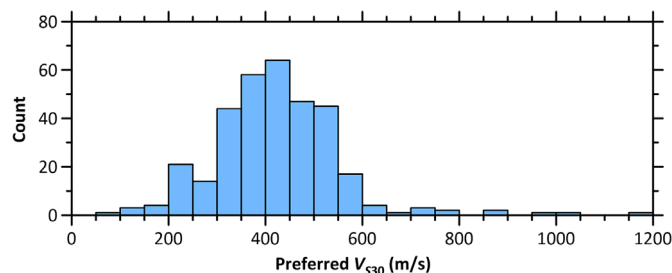
Figure 4. Histogram of V_{S30} recommended for analysis for the 333 accelerograph sites contributing data in this study. The color version of this figure is available only in the electronic edition.

Ground-Motion Data

A ground-motion database flatfile requires information on sources, recordings sites, and record-specific attributes (ground-motion parameters, processing details, and site-to-source distances). Previous sections have described source and site tables (Tables S1 and S2). This section describes the ground-motion selection and processing, intensity measure calculations, and database attributes. The ground-motion information is provided in the flatfile table, that is, Table S3.

Ground-motion selection and data processing

We consider data from earthquake events within the broader Aegean region, as defined in the Earthquake Source Database section. For those events, we consider recordings from the institutes comprising the HANs. To keep the size of the database at a manageable level while providing information of interest for GMPE development, we only consider events with **M** > 4 and recordings at distances <300 km. Shorter cutoff distances (approximately, 50–100 km) are used for events recorded by older analog and low-resolution digital instruments.
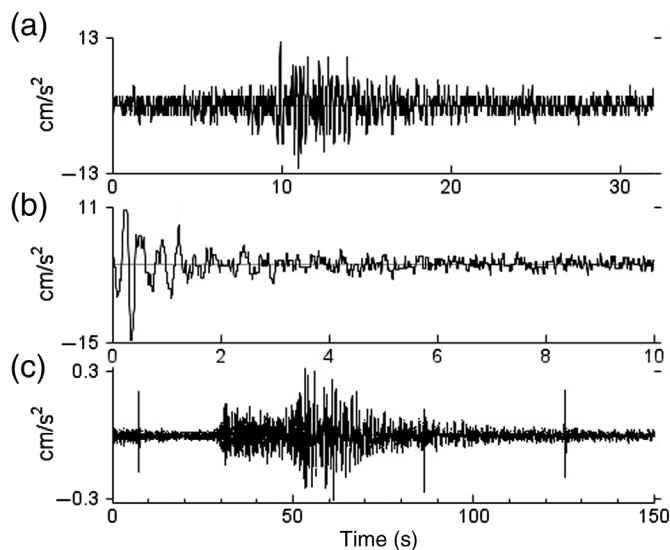
Figure 5. Examples of uncorrected accelerograms with various nonstandard errors in the time domain: (a) low digitizer resolution (vertical component of record ID: 862), (b) *S* trigger, and (c) anomalous high-frequency spikes (vertical component of record ID: 2753).

The procedures described here begin with digital versions of accelerograms. These are obtained directly from digital instruments, whereas, a digitization process is required for data from older analog instruments. We used digital versions of analog records developed in prior work (Margaris, 1986; Margaris *et al.*, 1989; Kalogeras, 2002; Skarlatoudis *et al.*, 2003, 2004; Theodoulidis *et al.*, 2004). The digital time series used in this work are publically available at data repositories listed in Data and Resources of this article.

A uniform data-processing procedure was applied to the digital records. This procedure is intended to screen out records that are unreliable for various reasons and to produce processed records with minimal effects of noise over a defined bandwidth. The processed records, in turn, are used for intensity measure calculations, as described in the next section. The general steps in the processing procedure are:

1. Visual screening to identify records with "nonstandard errors" that should be screened out (not used) or given special treatment during subsequent processing.
2. Windowing of records to identify the time intervals within which the earthquake sharking occurs.
3. Mean removal and low-cut filtering to reduce noise effects.

Visual screening of raw (digital but uncorrected) time series is applied to identify records with various issues (Douglas, 2003; Boore and Bommer, 2005), including low digitizer resolution relative to the signal amplitude (Fig. 5a), artificial cutoff of the records at the beginning (*S*-wave trigger, Fig. 5b) or end

(early termination of coda waves), and presence of high-frequency spikes with anomalously high accelerations (Fig. 5c). *S*-triggered accelerograms are eliminated. Records with low-digitizer resolution were flagged but were retained and processed in the standard manner (the impact of low resolution is to limit usable bandwidth). Records with anomalous spikes can be corrected with high-cut filters in some cases, and, if that is ineffective, the records are eliminated (Akkar *et al.*, 2010).

The windowing component of the procedure is intended to capture the time interval containing a measurable signal from the event. When records include multiple events, a time window encompassing as much signal as possible from the target event (generally largest in duration) is defined by eye. We sometimes use a Tukey window to taper the motion at the boundaries of the selected time interval; this is decided on a record-by-record basis. The windowing procedures applied in this study are admittedly subjective, but, they were consistently applied to all records by a single seismologist (first author). Experience suggests that the application of reasonable alternate windowing methods has relatively little effect on Fourier spectra and intensity measures in most cases (Akkar *et al.*, 2014).

Figure 6a shows an example of a signal with multiple late arrivals, likely associated with aftershocks (record ID: 1853, Earthquake_ID:1719; site GRE3). Two of these arrivals, at approximately 215 and 395 s, could be considered as having anomalous high-amplitude spikes. In the processing of this record, three windows were considered—full time series, 0–200 and 0–300 s. Figure 6b shows Fourier amplitude spectra for each of these time windows (prefiltering), which largely overlap up to the high-cut corner frequency. As a result, the effects of using alternate windows in this case are not significant. Ultimately, the processing of this record used a window from 0 to 200 s and a high-cut filter at 10 Hz, the effects of which are shown in Figure 6b.

Once records were screened and windowed, the mean over the pre-event portion of the record, if present, or over the whole record length, if not, was subtracted and a low-cut filtering procedure was applied. This procedure is intended to guide analysts toward selection of an optimal low-cut corner frequency f_c for each as-recorded component of ground motion. The procedure is presented by Boore (2001, 2005) and applied with some revision in the NGA projects (e.g., Ancheta *et al.*, 2014). As shown in the top plots in Figure 7, the procedure begins by plotting the uncorrected acceleration time series over the window length, along with integrations to velocity and displacement. The motion considered for this example (site ALM1, event 1507) has baseline drift in velocity and displacement, due to low-frequency noise. To remove these effects, the windowed accelerogram is zero padded at the beginning and at the end, to include the filter transient (the length of the pad depends on the filter corner frequency) and also to achieve a number of timesteps that is a power of two (e.g., 1024, 2048,
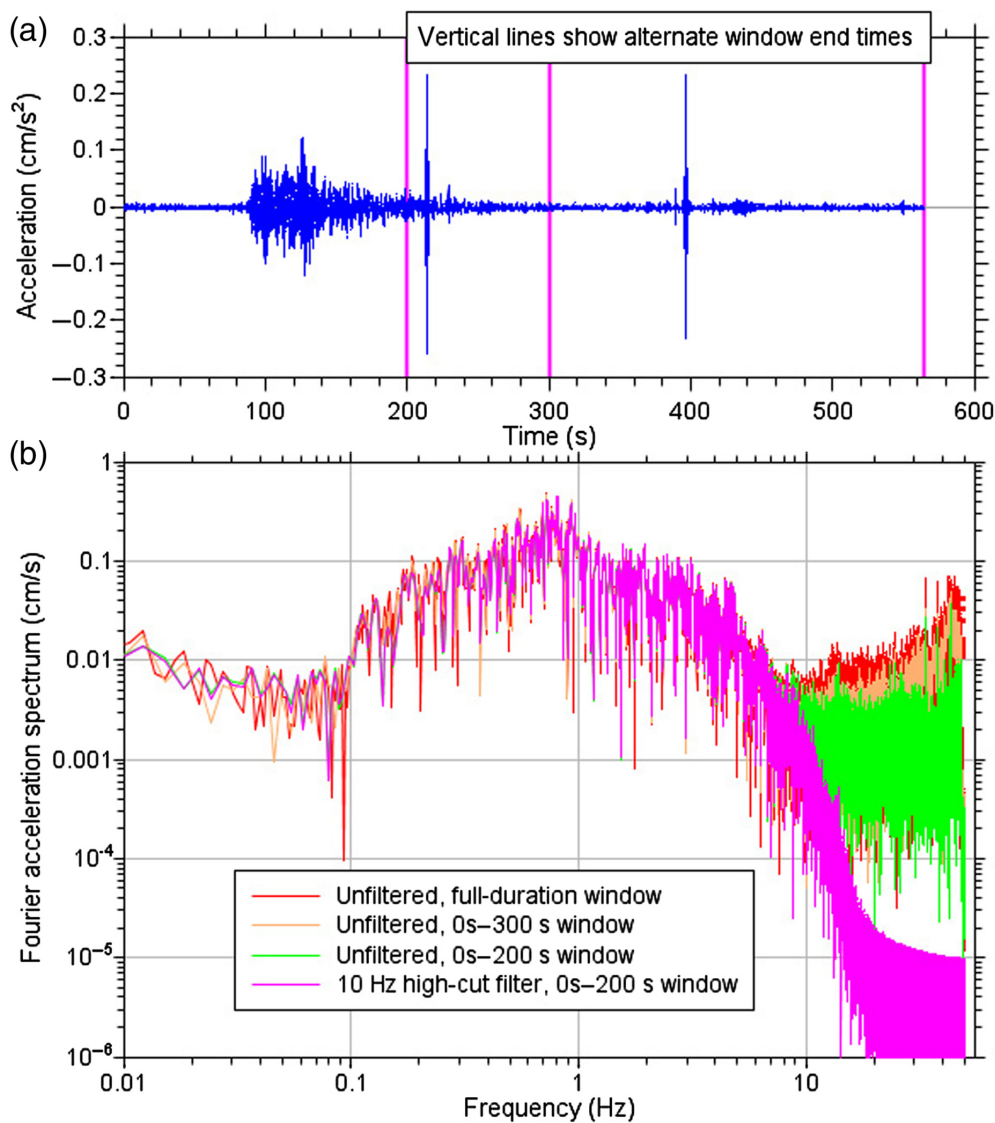
Figure 6. Recording at site GRE3 from event 1719, east–west component. (a) Time series with late-arriving short-duration motions (spikes) showing end times for alternate windows; (b) Fourier amplitude spectra for alternate windows and with application of a high-cut filter. The color version of this figure is available only in the electronic edition.

analysts provided nearly identical f_c-values. Where this was not the case, a consensus value was selected after some discussion. The final f_c-value selected for each component is provided in the flatfile table (Table S3). High-cut filters are applied only to most records from 2009 and later. Time-domain baseline correction of the filtered records was generally found to not be required. High-cut filters often have little impact on response spectra at short periods (e.g., Douglas and Boore, 2011).

Intensity measure calculations

Filtered accelerograms are used to compute intensity measures for the as-recorded azimuths and for alternate azimuths that provide different percentiles of the range in the horizontal plane. The intensity measures that are computed are peak ground acceleration (PGA), peak ground velocity, peak ground displacement (PGD), and 5% damped pseudospectral accelerations (PSAs) for 114 oscillator periods roughly equally spaced on a log scale from 0.01 to 20 s. PSA values are provided at all selected oscillator periods, regardless of f_c-values. PEER-NGA protocols recommend that spectral ordinates should not be used for oscillator periods longer than $1/(1.25f_c)$ (Ancheta *et al.*, 2014). We recommend following these protocols with the Hellenic dataset as well. The PGD values arguably should not be used, because they are especially sensitive to the low-cut corner frequencies.

The procedure used to compute intensity measures for alternate azimuths that provide different percentiles of the range in the horizontal plane was presented by Boore (2010). The intensity measures computed using this process are described using RotD*nn* notation, in which *nn* represents the percentile. We provide in the flatfile (Table S3), the RotD50 (median component) intensity measures. Records with only one horizontal component are precluded from the dataset.
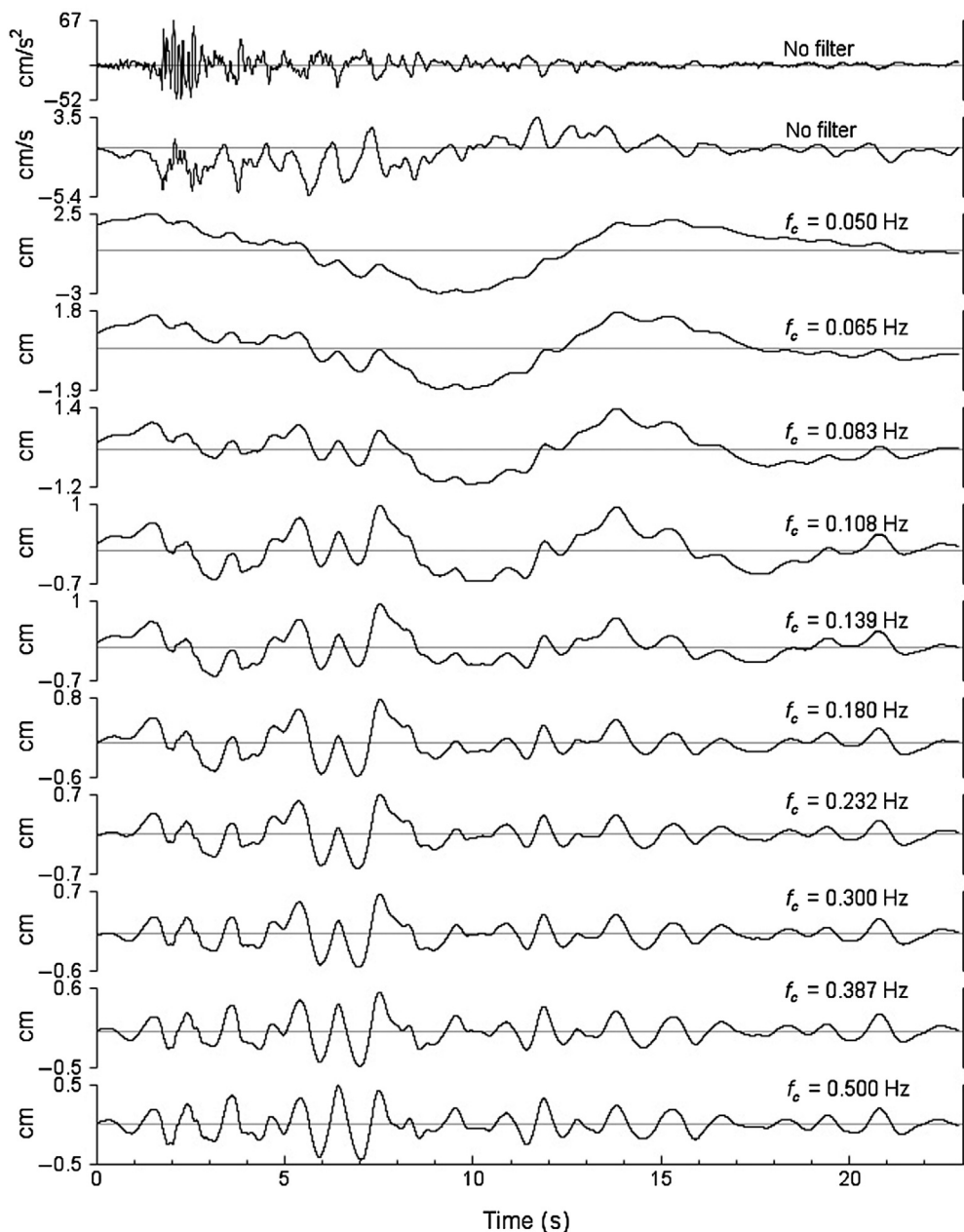
4096, etc.). Acausal low-cut Butterworth filters of sufficient order are then applied to achieve a specified asymptotic behavior at low frequencies (usually f^8 (Boore, 2005) for 10 cut frequencies (f_c-values) logarithmically equally spaced in three groups: 0.05–0.5, 0.1–1, and 0.5–5Hz (a total of 30 f_c-values are considered). The filtered accelerograms are then double integrated to displacement, the results of which are shown for the 0.5–5 Hz group in Figure 7. The results are visually inspected by three analysts, each of which selects an f_c-value that produces a stable displacement time series (without baseline drift) and with the minimal possible reduction of amplitudes. This procedure used several time-series processing routines from Boore (2012). In most cases, the three

Figure 7. Time series for the *L*-component record at ALM1 site during event 1507 (1980 **M** 5.2 Almyros, recorded at $R_{RUP} = 26$ km), showing acceleration and velocity for the unfiltered record (top three plots) and displacement histories following application of low-cut filters at various f_c-values (logarithmically equally spaced) from 0.05 to 0.50 Hz. The displacement time series have been stripped of the pads added for the filtering, which is why the beginning of the plotted time series sometimes do not start at 0.0.

Database attributes

The ground-motion flatfile compiled for this project (Table S3) contains the computed intensity measures, event information from the source table, site information from the site table, and various site-to-source distance parameters. Details on the information provided are given in preceding sections of this article.

Figure 9 shows the cumulative number of events (with ≥2 records) and recordings in the database as a function of time. Approximately, 50% of the seismic events occurred since 2005, producing 85% of the records. Greece has not become more seismically active during this period, rather we have more information on the earthquakes that occur as a result of the increased number of high-resolution (24-bit) digital accelerographs that have been installed since 2008 (Margaris *et al.*, 2014).

Figure 10 shows the distribution of records in magnitude–rupture distance space for PGA (all unscreened records represented) and 5.0 s PSA (some records are not shown because 5.0 s is beyond the usable period range). For PGA, there are 2993 recordings from 471 events. The database is well populated for the 10–300 km distance range, for magnitudes between about 4 and 7. The maximum distance for **M** 4.0– 4.8 is approximately 150 km. There are very few recordings at rupture distances under about 5 km. The data distributions in Figure 10 generally overlap with the data distribution in figure 2 of Luzi *et al.* (2016) for the ESM database, with two exceptions: (1) the ESM database extends to larger magnitudes (upper bound of 7.4) and (2) the Hellenic database contains data out to distances of 300 km for events with magnitudes as low as 4.8, whereas, the ESM database extends to 300 km, starting at **M** 6.

Figure 8 shows the effect of the filter corners on the number of usable recordings and number of usable events (based on a minimum criterion of two or more recordings per event), as a function of oscillator period. The fall-off beyond about 1.0–3.0 s (most appreciable at 5 s) occurs, because some records (especially, those from older instruments) required relatively high f_c-values in the range of 0.2–1.0 Hz.
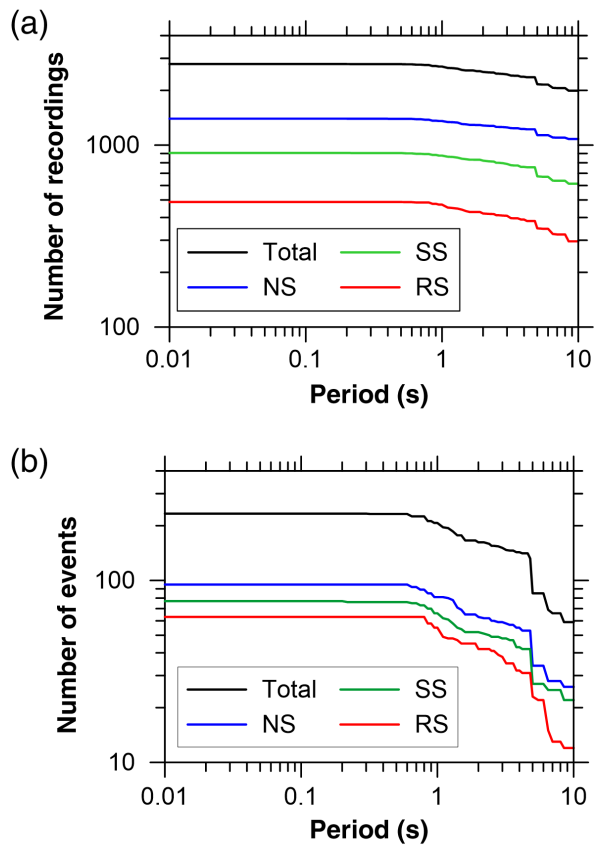
Figure 8. Number of (a) usable recordings and (b) events as a function of oscillator period (data for events without focal mechanism removed, total recordings plotted is 2791). NS, normal slip; RS, reverse slip; SS, strike slip. The color version of this figure is available only in the electronic edition.
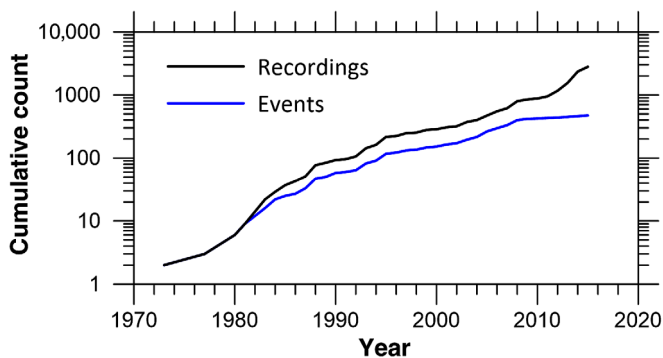

Figure 9. Cumulative numbers of recordings and events (having at least two recordings) since 1972. The color version of this figure is available only in the electronic edition.

Figure 11 illustrates some attributes of events with at least two recordings for PGA. Each event is classified as strike slip, reverse, or normal, as per the criteria given in the FPSs section, and, is represented by a point in the figure as a function of
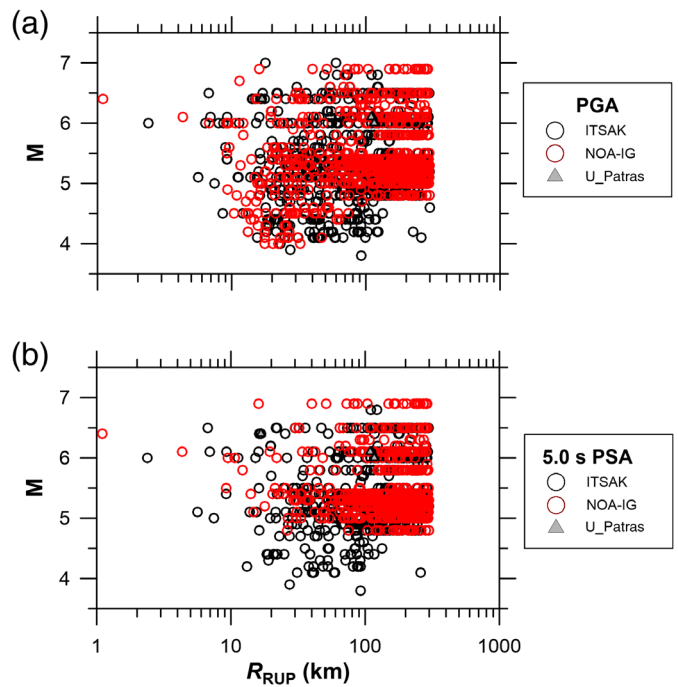

Figure 10. Distributions of the Hellenic Strong Motion Data in M-R_{RUP} space for (a) peak ground acceleration (PGA) and (b) 5.0 s pseudospectral acceleration (PSA). NOA-IG, NOA–Geodynamic Institute; R_{RUP}, closest distance to rupture plane. The color version of this figure is available only in the electronic edition.
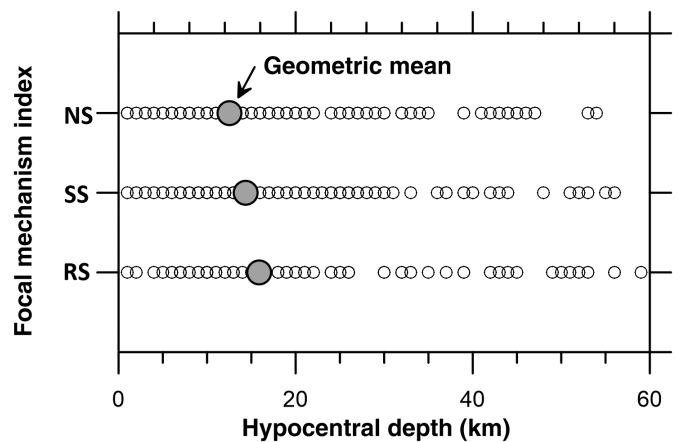

Figure 11. Dependence of event hypocentral depth on focal mechanism.

hypocentral depth. Most of seismic events (70%) are shallow crustal (depths <30 km). Events at greater depth may be related to subduction tectonic processes; we have not attempted to remove such events from this dataset, aside from application of the 60 km depth limit. As mentioned previously, users of the database may wish to screen the data based on shallower hypocentral depth, to minimize the potential for

subduction events being in the analyzed dataset. Faulting types are predominantly strike slip and normal (38% and 37%, respectively), whereas the balance are reverse (25%). Focal depths tend to be shallower for normal-slip events (geometric mean 12.5 km) than for strike-slip or reverse events (14.3 and 15.9 km, respectively).

Summary and Conclusions

In this article, we describe a database of Hellenic ground motions and supporting seismic source and recording site metadata. The result of a long-term Greece–Unites States collaboration, this database supersedes and significantly updates earlier Hellenic databases (HEllenic Accelerogram Database [HEAD]; Theodoulidis et al., 2004; GHEAD, see Data and Resources). The main advantages of this database relative to prior data compilations for Greece are (1) uniformly processed ground motions with identified maximum usable periods; (2) significantly enhanced database size, including substantially more recordings per event and per site; (3) improved and uniformly applied protocols for metadata assignment, including magnitudes, distances, and site parameters. We encourage the incorporation of this expanded and quality-enhanced database in future European and global ground-motion databases.

Earthquake source information was compiled from bulletins and catalogs maintained by various national and ISCs, as well as from research articles and reports. Moment tensor solutions derived from broadband instrumental recordings were available for most of the events, providing estimates of source location, seismic moment, moment magnitude, FPSs, and rake angles. For a few selected earthquakes, additional finite-fault source parameters, such as along-strike length, down-dip width, and depth to top of rupture are provided. Site parameters have been substantially updated with V_{S30}-values assigned to each of the 333 sites that have produced usable recordings, approximately, 1/3 of which have been characterized based on on-site geophysical measurements, with the remainder estimated using proxy-based V_{S30} prediction equations. A source table and site table presenting the compiled information are included in Tables S1–S2.

Using source and site locations, we have estimated various distance metrics for each recording, including metrics that account for fault dimensions (rupture distance and distance to surface projection of fault). Finite-fault models are used for this purpose where available; otherwise, simulation-based methods are used.

The database includes strong-motion data from 471 shallow-crustal earthquakes that have occurred in the broader Aegean area for the period 1973–2015, with magnitudes $3.8 \leq \mathbf{M} \leq 7.0$ and rupture distance ≤300 km. The database includes 2993 three-component acceleration time histories, most from digital high-resolution instruments. Limitations of the database for ground-motion modeling purposes include: (1) limited data for large magnitudes ($\mathbf{M} \gtrsim 6.5$), (2) lack of data for close distances ($\lesssim 5$ km) for all magnitudes, (3) limited data at large distances (>100 km) for small magnitudes ($\mathbf{M} < 4.8$), and (4) limited data from hard-rock and soft-soil sites ($V_{S30} > 650$ and <200 m/s, respectively). Future improvement of the Hellenic strong motion database is anticipated, especially, with regard to expanding in situ site characterization at recording sites.

This database has been used to develop a regional customization of global GMPEs for Greece (Boore et al., 2020), will likely be used for future European ground-motion model development, and should also be useful for engineering applications, such as time-series selection for response-history analyses.

Data and Resources

Source data resources accessed in this work are from earthquake catalogs and the literature. These sources are cited for each event in the source table in the supplemental material. The earthquake catalogs noted in the Earthquake Locations section, when International Seismological Centre (ISC) bulletins are not used, can be found at the following URLS: National Earthquake Information Center (NEIC) (Preliminary Determination of Epicenter [PDE]; ftp://hazards.cr.usgs.gov/NEICPDE), online bulletins from Aristotle University of Thessaloniki (AUTh; http://geophysics.geo.auth.gr/ss/station_index_en.html), and online earthquake catalog of the National Observatory of Athens (NOA, http://www.gein.noa.gr/en/seismicity/earthquake-catalogs). Site data resources accessed in this work are as described in a previous article (Stewart et al., 2014). Individual data sources for each site are listed in the site table in the supplemental material. The Institute of Geology and Mine Exploration (IGME) resources referenced in the Site Parameters section are available at https://www.igme.gr/geoportal/. All of the ground-motion intensity measures and processing are contained in the flatfile table in the supplemental material. The digital acceleration time series used in this work are available from repositories maintained by Institute of Engineering Seismology and Earthquake Engineering ITSAK (http://www.itsak.gr/smdata/) and NOA (https://accelnet.gein.noa.gr/sm_data). Each repository contains the same sets of time series. Information about Geographic Information System (GIS) HEllenic Accelerogram Database (GHEAD) database is available at http://ghead.itsak.gr/map/. All websites were last accessed in February 2021. The source and site tables developed in this article are provided as supplemental material in Tables S1 and S2. The project flatfile is provided as Table S3.

Acknowledgments

References

Aki, K., and P. Richards (1980). *Quantitative Seismology, Theory and Methods*, Vols. I and II, W. H. Freeman, San Francisco, California.

Akkar, S., Z. Cagnan, E. Yerien, O. Erdogan, M. A. Sandikkaya, and P. Gulkan (2010). The recent compiled Turkish strong motion database: Preliminary investigation for seismological parameters, *J. Seismol.* **14,** 457–479.

Akkar, S., M. A. Sandikkaya, M. Senyurt, A. A. Sisi, B. O. Ay, R. Traversa, J. Douglas, F. Cotton, L. Luzi, B. Hernandez, *et al.* (2014). Reference database for seismic ground motion in Europe (RESORCE), *Bull. Earthq. Eng.* **12,** 311–339.

Ambraseys, N. N., J. Douglas, R. Sigbjönsson, C. Berge-Thierry, P. Suhadoic, G. Costa, and P. Smit (2004). Dissemination of European strong motion data, Vol. 2, *Proc. 13th World Conf. Earthquake Engineering*, Vancouver, British Columbia.

Ambraseys, N. N., P. Smit, R. Beradi, D. Rinaldis, F. Cotton, and C. Berge-Thierry (2000). *Dissemination of European Strong-Motion Data*, CD-ROM collection, European Commission, Directorate General XII, Science, Research and Development, Environment and Climate Program, Brussels, Belgium.

Ambraseys, N. N., P. Smit, J. Douglas, B. Margaris, R. Sigbjönsson, S. Olafsson, P. Suhadoic, and G. Costa (2004). Internet site for European strong motion data, *Boll. Geof. Teor. Appl.* **45,** 113–129.

Ancheta, T. D., R. B. Darragh, J. P. Stewart, E. Seyhan, W. J. Silva, B. S.-J. Chiou, K. E. Wooddell, R. W. Graves, A. R. Kottke, D. M. Boore, *et al.* (2014). NGA-West 2 database, *Earthq. Spectra* **30,** 989–1005.

Baba, A. B., E. E. Papadimitriou, B. C. Papazachos, C. A. Papaioannou, and B. G. Karakostas (2000). Unified local magnitude scale for earthquakes of south Balkan area, *Pure Appl. Geophys.* **157,** 765–783.

Benetatos, C., D. Dreger, and A. Kiratzi (2007). Complex and segmented rupture associated with the 14 August 2003 M_w 6.2 Lefkada, Ionian Islands, earthquake *Bull. Seismol. Soc. Am.* **97,** no. 1B, 35–51.

Benetatos, C., A. Kiratzi, Z. Roumelioti, G. Stavrakakis, G. Drakatos, and I. Latoussakis (2005). The 14 August 2003 Lefkada Island (Greece) earthquake: Focal mechanisms of the mainshock and of the aftershock sequence, *J. Seismol.* **9,** 171–190.

Berckhemer, H., and K. Hsu (Editors) (1982). *Alpine-Mediterranean Geodynamics,* , Geodynamic Series, Vol. 7, American Geophysical Union, Washington D.C.

Bernard, P., P. Briole, B. Meyer, H. Lyon-Caen, J.-M. Gomez, C. Tiberi, C. Berge, R. Cattin, D. Hatzfeld, C. Lachet, *et al.* (1997). The M_s = 6.2, June 15, 1995 Aigion earthquake (Greece): Evidence for low angle normal faulting in the Corinth rift, *J. Seismol.* **1,** no. 2, 131–150.

Boore, D. M. (2001). Effect of baseline corrections on displacement and response spectra for several recordings of the 1999 Chi-Chi, Taiwan, earthquake, *Bull. Seismol. Soc. Am.* **91,** 1199–1211.

Boore, D. M. (2005). On pads and filters: Processing strong-motion data, *Bull. Seismol. Soc. Am.* **95,** 745–750.

Boore, D. M. (2010). Orientation-Independent, non geometric-mean measures of seismic intensity from two horizontal components of motion, *Bull. Seismol. Soc. Am.* **100,** 1830–1835.

Boore, D. M. (2012). TSPP—A collection of FORTAN programs for processing and manipulating time series, *U.S. Geol. Surv. Open-File Rept. 2008-1111,* 47 pp.

Boore, D. M., and G. M. Atkinson (2007). Boore–Atkinson NGA ground motion relations for the geometric mean horizontal component of peak and spectral ground motion parameters, *PEER Report 2007/01,* Pacific Earthquake Engineering Research Center, University of California, Berkeley, California, 234 pp.

Boore, D. M., and J. J. Bommer (2005). Processing of strong-motion accelerograms: Needs, options and consequences, *Soil Dynam. Earthq. Eng.* **25,** 93–115.

Boore, D. M., J. P. Stewart, A. A. Skarlatoudis, E. Seyhan, B. Margaris, N. Theodoulidis, E. Scordilis, I. Kalogeras, N. Klimis, and N. S. Melis (2020). A ground-motion prediction model for shallow crustal earthquakes in Greece, *Bull. Seismol. Soc. Am.* doi: 10.1785/0120200270.

Bozorgnia, Y., N. A. Abrahamson, L. Al Atik, T. D. Ancheta, G. M. Atkinson, J. W. Baker, A. Baltay, D. M. Boore, K. W. Campbell, B. S.-J. Chiou, *et al.* (2014). NGA-West2 research project, *Earthq. Spectra* **30,** 973–987.

Carver, D., and G. A. Bollinger (1983). Distribution of the seismicity related to the June 20, 1978, M_s = 6.5 northern Greece earthquake, in *The Thessaloniki, Northern Greece, Earthquake of June 20, 1978 and its Seismic Sequence*, B. C. Papazachos and P. G. Carydis (Editors), Technical Chamber of Greece, Section of Central Macedonia, 133–149.

Chiou, B. S. J., and R. R. Youngs (2008). NGA model for average horizontal component of peak ground motion and response spectra, *PEER Report 2008/09,* Pacific Engineering Research Center, University of California, Berkeley, 293 pp.

Contreras, V., J. P. Stewart, T. Kishida, R. B. Darragh, B. S. J. Chiou, S. Mazzoni, N. Kuehn, S. K. Ahdi, K. Wooddell, R. R. Youngs, *et al.* (2020). Chapter 4: Source and path metadata, in data resources for NGA-Subduction project, *PEER Report 2020/02,* J. P. Stewart (Editor), Pacific Earthquake Engineering Research Center, University of California, Berkeley, Berkeley, California, 41–112.

Dogan, B., T. S. Irmak, A. Karakas, and D. Kalafat (2016). Seismotectonic content by the source parameters of the 10 June 2012 Oludeniz–Fethiye (Dodecanese Islands) M_w 6.1 earthquake and aftershocks (southwestern Turkey), *Acta Geod. Geophys.* **51,** 15–41.

Douglas, J. (2003). What is a poor quality strong-motion record? *Bull. Earthq. Eng.* **1,** 141–156.

Douglas, J., and D. M. Boore (2011). High-frequency filtering of strong-motion records, *Bull. Earthq. Eng.* **9,** 395–409.

Duni, L., S. Kuka, and N. Kuka (2010). Local relations for converting M_L to M_w in southern–western Balkan region, *Acta Geod. Geophys.* **45,** no. 3, 317–323.

Dziewonski, A. M., T.-A. Chou, and J. H. Woodhouse (1981). Determination of earthquake source parameters from waveform data for studies of global and regional seismicity, *J. Geophys. Res.* **86,** 2825–2852, doi: 10.1029/JB086iB04p02825.

Ekström, G., M. Nettles, and A. M. Dziewonski (2012). The Global CMT project 2004–2010: Centroid-moment tensors for 13,017 earthquakes, *Phys. Earth Planet. In.* **200/201,** 1–9, doi: 10.1016/j.pepi.2012.04.002.

European Committee for Standardization (CEN) (2004). Eurocode 8: Design of structures for earthquake resistance—Part 1: General rules, seismic actions and rules for buildings, *I.S. EN 1998-1:2004.*

Galanis, O. (2010). Contribution to the development and implementation of algorithms for earthquake location and seismic tomography, *Ph.D. Thesis,* Aristotle University of Thessaloniki, Greece, 317 pp. (in Greek).

Gardner, J. K., and L. Knopoff (1974). Is the sequence of earthquakes in southern California with aftershocks removed, Poissonian? *Bull. Seismol. Soc. Am.* **64,** 1363–1367.

Gasperini, P., B. Lolli, G. Vannucci, and E. Boschi (2012). A comparison of moment magnitude estimates for the European–Mediterranean and Italian regions, *Geophys. J. Int.* **190,** 1733–1745.

Gorgun, E. (2017). Source mechanisms and stress fields of the 15–16 June 2013 Crete earthquake sequence along Hellenic subduction zone, *Pure Appl. Geophys.* **174,** 1181–1199.

Goulet, C. A., T. Kishida, C. H. Cramer, R. B. Darragh, W. J. Silva, Y. M. A. Hashash, J. Harmon, J. P. Stewart, K. Wooddell, and R. R. Youngs (2014). PEER NGA-East database, *PEER Report 2014/17,* Pacific Earthquake Engineering Research Center, University of California, Berkeley, Berkeley, California.

Hanks, T. C., and H. Kanamori (1979). A moment magnitude scale, *J. Geophys. Res.* **84,** 2348–2350.

Howell, A., K. Palamartchouk, X. Papanikolaou, D. Paradissis, C. Raptakis, A. Copley, P. England, and J. Jackson (2017). The 2008 Methoni earthquake sequence: The relationship between the earthquake cycle on the subduction interface and coastal uplift in SW Greece, *Geophys. J. Int.* **208,** 1592–1610.

Iwahashi, J., and R. J. Pike (2007). Automated classifications of topography from DEMs by an unsupervised nested-means algorithm and a three-part geometric signature, *Geomorphology* **86,** 409–440.

Kalogeras, I. S. (2002). A strong motion database in Greece, *Nat. Hazards* **26,** 265–277.

Karakaisis, G. F., C. B. Papazachos, and E. M. Scordilis (2010). Seismic sources and main seismic faults in the Aegean and surrounding area, *Bull. Geol. Soc. Greece,* **XLIII,** no. 4, 2026–2042.

Karakostas, V., K. Mirek, M. Mesimeri, E. Papapdimitriou, and J. Mirek (2017). The aftershock sequence of the 2008 Achaia, Greece, earthquake: Joint analysis of seismicity relocation and persistent scatterers interferometry, *Pure Appl. Geophys.* **174,** 151–176.

Karakostas, V., E. Scordilis, C. Papaioannou, B. Papazachos, and D. Mountrakis (1993). Focal properties of the October 16, 1988 Killini earthquake (western Greece), *Proc. of the 2nd Congress of the Hellenic Geophysical Union,* Florina, Greece, 5–7 May, 136–145.

Kiratzi, A. A. (2016). The 16 April 2015 M_w 6.1 earthquake sequence near Kasos Island at the eastern Hellenic subduction zone, *Bull. Geol. Soc. Greece* **50,** 1163–1173.

Konstantinou, K. I. (2015). Moment magnitude estimates for earthquakes in the Greek region: A comprehensive comparison, *Bull. Seismol. Soc. Am.* **105,** 2555–2562.

Kuehn, N. M., and N. A. Abrahamson (2018). The effect of uncertainty in predictor variables on the estimation of ground-motion prediction equations, *Bull. Seismol. Soc. Am.* **108,** 358–370.

LePichon, X., and J. Angelier (1979). The Hellenic arc and trench system: A key to the neotectonic evolution of the eastern Mediterranean area, *Tectonophysics* **60,** 1–42.

Luzi, L., R. Puglia, E. Russo, M. D'Amico, C. Felicetta, F. Pacor, G. Lanzano, U. Çeken, J. Clinton, G. Costa, *et al.* (2016). The engineering strong-motion database: A platform to access Pan-European accelerometric data, *Seismol. Res. Lett.* **87,** 987–997.

Lyon-Caen, H., R. Armijio, J. Drakopoulos, J. Baskoutas, N. Delibasis, R. Gauloni, V. Kouskouna, J. Latoussakis, K. Makropoulos, P. Papapdimitriou, *et al.* (1988). The 1986 Kalamata (South Peloponnesus) earthquake: Detailed study of a normal fault, evidences for east–west extension in the Hellenic arc, *J. Geophys. Res.* **93,** 14,967–15,000.

Margaris, B. (1986). Digitizing errors and filters, *Report 86-03,* Institute of Engineering Seismology and Earthquake Engineering, Thessaloniki, Greece, 43 p., doi: 10.6084/m9.figshare.14135603.v1.

Margaris, B., I. Kalogeras, C Papaioannou, A. Savvaidis, and N. Theodoulidis (2014). Evaluation of the national strong motion network in Greece: Deployment, data-processing and site characterization, *Bull. Earthq. Eng.* **12,** 237–254.

Margaris, B., D. Papastamatiou, and N. Theodulidis (1989). ITSAK: Strong motion data processing, *Report: 89-02,* Institute of Engineering Seismology and Earthquake Engineering, Thessaloniki, Greece, 27 pp., doi: 10.6084/m9.figshare.14135585.v1.

Pacific Earthquake Engineering Research center (PEER) (2020). *Data resources for NGA-Subduction Project, PEER Report 2020/02,* Bozorgnia, Y. and J. P. Stewart (Editors), University of California, Berkeley, Berkeley, California, 162 pp.

Papadimitriou, P., N. Voulgaris, I. Kassaras, G. Kaviris, N. Delibasis, and K. Makropoulos (2002). The $M_w = 6.0$, 7 September 1999 Athens earthquake, *Nat. Hazards* **27,** 15–33.

Papadopoulos, G. A., G. Drakatos, D. Papanastassiou, I. Kalogeras, and G. Stavrakakis (2000). Preliminary results about the catastrophic earthquake of 7 September 1999 in Athens, Greece, *Seismol. Res. Lett.* **71,** 318–329.

Papazachos, B., P. Comninakis, E. Papadimitriou, and E. Scordilis (1984). Properties of the February–March 1981 seismic sequence in the Alkyonides gulf of central Greece, *Ann. Geophys.* **2,** 537–544.

Papazachos, B., A. Kiratzi, B. Katakostas, D. Panagiotopoulos, E. Scordilis, and D. Moundrakis (1988). Surface fault traces, fault plane solution and spatial distribution of the aftershocks of the September 13, 1986 earthquake of Kalamata (southern Greece), *Pure Appl. Geophys.* **126,** 55–68.

Papazachos, B., and C. Papazachou (2003). *The Earthquakes of Greece,* Ziti Publications, Thessaloniki, Greece, 317 pp. (in Greek).

Papazachos, B. C., and P. E. Comninakis (1971). Geophysical and tectonic features of the Aegean arc, *J. Geophys. Res.* **76,** 8517–8533.

Papazachos, B. C., A. A. Kiratzi, and B. G. Karacostas (1997). Toward a homogeneous moment-magnitude determination for earthquakes in Greece and the surrounding area, *Bull. Seismol. Soc. Am.* **87,** 474–483.

Papazachos, B. C., E. M. Scordilis, D. G. Panagiotopoulos, C. B. Papazachos, and G. F. Karakaisis (2004). Global relations between seismic fault parameters and moment magnitude of earthquakes, *Bull. Geol. Soc. Greece* **XXXVI,** 1482–1489.

Rigo, A., J.-B. de Chabalier, B. Meyer, and R. Armijo (2004). The 1995 Kozani–Grevena (northern Greece) earthquake revisited: An improved faulting model from synthetic aperture radar interferometry, *Geophys. J. Int.* **157,** 727–736.

Roumelioti, Z., C. Benetatos, and A. Kiratzi (2009). The 14 February 2008 earthquake (M 6.7) sequence offshore south Peloponnese (Greece): Source models of the three strongest events, *Tectonophysics* **471,** 272–284.

Roumelioti, Z., D. Dreger, A. Kiratzi, and N. Theodoulidis (2003). Slip distribution of the 7 September 1999 Athens earthquake inferred from an empirical Green's function study, *Bull. Seismol. Soc. Am.* **93,** 775–782.

Roumelioti, Z., A. Kiratzi, and D. Dreger (2004). The source process of the 2001 July 26 Skyros Island (Greece) earthquake, *Geophys. J. Int.* **156,** 541–548.

Saltogianni, V., M. Gianniou, T. Taymaz, S. Yolsal-Çevikbilen, and S. Stiros (2016). The 2014 M_w 6.9 North Aegean trough (NAT) earthquake: Seismological and geodetic evidence, *Bull. Geol. Soc. Greece* **50,** no. 3, 1583–1592.

Saltogianni, V., T. Taymaz, S. Yolsal-Çevikbilen, T. Eken, F. Moschas, and S. Stiros (2017). Fault model for the 2015 Leucas (Aegean arc) earthquake: Analysis based on seismological and geodetic observations, *Bull. Seismol. Soc. Am.* **107,** 433–444.

Scordilis, E. M. (2005). Globally valid relations converting M_s, m_b and MJMA to M_w, *NATO Advanced Research Workshop on Earthquake Monitoring and Seismic Hazard Mitigation in Balkan Countries*, Book of Abstracts, Borovetz-Rila Mountain, Bulgaria, 11–17 September, 158–161.

Scordilis, E. M. (2006). Empirical global relations converting M_S and m_b to moment magnitude, *J. Seismol.* **10,** 225–236.

Skarlatoudis, A. A., C. B. Papazachos, B. N. Margaris, N. P. Theodoulidis, C. P. Papaioannou, I. Kalogeras, E. M. Scordilis, and V. G. Karakostas (2003). Empirical peak ground-motion predictive relations for shallow earthquakes in Greece, *Bull. Seismol. Soc. Am.* **93,** 2591–2603.

Skarlatoudis, A. A., N. Theodoulidis, C. Papaioannou, and Z. Roumelioti (2004). The dependence of the peak horizontal acceleration on magnitude and distance for small magnitude earthquakes in Greece 2004, *Proc. 13th World Conf. Earthquake Engineering*, Vancouver, Canada, 1–6 August, Paper Number 1857.

Sokos, E., A. Kiratzi, F. Gallovič, J. Zahradník, A. Serpetsidaki, V. Plicka, J. Janský, J. Kostelecký, and G.-A. Tselentis (2015). Rupture process of the 2014 Cephalonia, Greece, earthquake doublet (M_w 6) as inferred from regional and local seismic data, *Tectonophysics* **656,** 131–141.

Stewart, J. P. (2000). Variations between foundation-level and free-field earthquake ground motions, *Earthq. Spectra* **16,** 511–532.

Stewart, J. P., N. Klimis, A. Savvaidis, N. Theodoulidis, E. Zargli, G. Athanasopoulos, P. Pelekis, G. Mylonakis, and B. Margaris (2014). Compilation of a local V_S profile database and its application for inference of V_{S30} from geologic and terrain-based proxies, *Bull. Seismol. Soc. Am.* **104,** 2827–2841.

Theodoulidis, N., I. Kalogeras, C. B. Papazachos, V. Karastathis, B. N. Margaris, C. Papaioannou, and A. A. Skarlatoudis (2004). HEAD v1.0: A Unified HEllenic Accelerogram database, *Seismol. Res. Lett.* **75,** 36–45.

Tsampas, A. (2006). The critical earthquake model in low seismicity areas of Europe, *M.Sc. Thesis*, Aristotle University of Thessaloniki, 135 pp. (in Greek).

Wessel, P., and W. H. F. Smith (1995). New version of Generic Mapping Tools released, *Eos Trans. AGU* **76,** 697–723.